ments.[6] Also, it has a rather high Q which offers advantages of lower loss and narrow-band design as desired.

A plot of Q_p (loaded Q) vs. capacitive coupling slot size is given in Fig. 5. This represents measured data taken on a single-section filter.

Figure 6 shows the measured and computed (lossless case) insertion loss of a single-section filter vs. frequency for both states of the switch. From the measured insertion loss at band center and (2), the unloaded Q_u can be estimated. These measurements should be made for both the forward and the reverse bias conditions. With this data, it is possible to design and meet many different switching specifications.

[6] Hunton, J. K., and A. G. Ryals, Microwave variable attenuators and modulators using PIN diodes, *IRE Trans. on Microwave Theory and Techniques*, vol MTT-10, Jul 1962, pp 262–273.

Figure 7 shows the attenuation characteristics of a four-section equal Q filter switch for both conditions of switching while Fig. 8 shows the reflection loss. It is to be noted that the attenuation is in excess of 80 dB for a bandwidth of 10 Mc/s in the reject band, and that the insertion loss in the pass band at a frequency displacement of 120 Mc/s is less than 0.5 dB. Measurements of switching time show it to be less than 1 μs.

When the characteristics of this switch operating under 8 watts of RF power were checked over a temperature range of plus 65°C to minus 10°C, there was no change measured in response or loss attributable to the diodes.

Acknowledgments

The authors acknowledge the contributions of R. E. Neidert relative to switch evaluation under conditions of high power and changing temperature.

A High-Power Ferroelectric Limiter

M. COHN, SENIOR MEMBER, IEEE, AND A. F. EIKENBERG

Abstract—**Ferroelectric limiters capable of handling peak input power levels in excess of 25 kW with a small signal insertion loss of 0.5 dB have been built. The measured performance and a theoretical analysis have shown that excellent limiting characteristics can be obtained, and that saturation power output levels ranging from a few watts up to megawatts can be obtained with ferroelectric pellets that can be conveniently fabricated. The limited available material data indicates that ferroelectric limiters will offer their greatest advantage in the HF, VHF, and UHF bands. The theoretical analysis of the expected temperature rise within the ferroelectric pellet has shown that, by proper design, very-high-average power levels also can be handled. A recovery time of less than ten microseconds has been measured.**

Introduction

A NEW TYPE of solid state high-power limiter, which utilizes the large signal nonlinear characteristics of ferroelectric materials, has been developed. Since the nonlinear action takes place within a bulk ceramic material, the high-power handling capability was expected. However, a deterrent to the use of ferroelectric materials in devices such as high-power limiters is the lack of sufficient data on the electrical properties of these materials. This is particularly true in the case of their large signal properties, knowledge of which is essential in order to design and predict the performance of limiters.

Manuscript received July 29, 1964; revised October 19, 1964. The research for this work was sponsored by the Navy Department, Bureau of Ships, Electronics Division under Contract NObsr-87394.

The authors are with the Advanced Technology Corporation (formerly the Research Division of Electronic Communications, Inc.), Timonium, Md.

Properties of the Ferroelectric Material

The ferroelectric material used was a ceramic mixture of 45 per cent lead titante and 55 per cent strontium titanate. This mixture is referred to in mole per cent. Its small signal electrical properties were determined from measurements made on a small circular parallel-plate capacitor. This small ferroelectric capacitor (diameter = 0.033 inch, height = 0.050 inch) was located between the end of the center conductor and an end plate of a special coaxial holder. A diagram of the measurement system is shown in Fig. 1. A heating coil was placed around that portion of the coaxial holder containing the ferroelectric capacitor. A thermocouple was used to monitor temperature. Direct current voltage, up to 2000 volts, could be applied across the plates of the ferroelectric capacitor.

The small signal dielectric constant (K) and dielectric loss tangent of the 45 per cent $PbTiO_3$–55 per cent $SrTiO_3$ ceramic material were measured as a function of temperature (T) at a frequency of 218 Mc/s. The dielectric constant values were determined from standard input impedance measurements made with a slotted line. The loss tangent was measured using a cavity

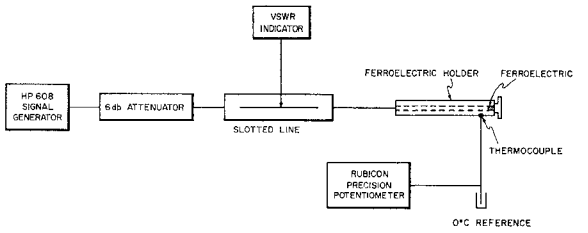

Fig. 1. Measurement of ferroelectric properties.

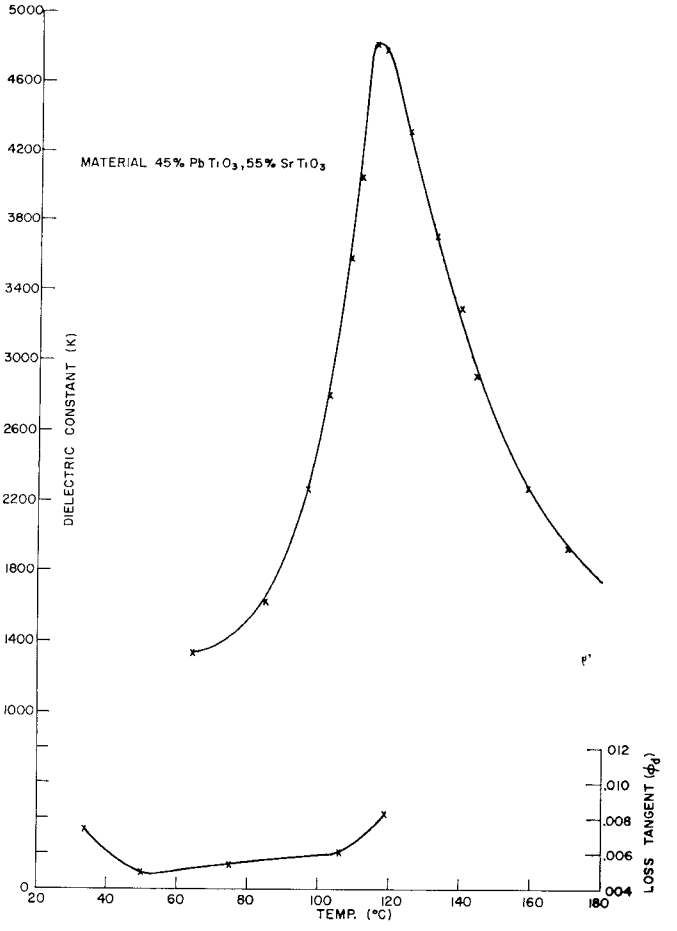

Fig. 2. Loss tangent and dielectric constant vs. temperature.

resonator. Curves of the dielectric constant and loss tangent as a function of temperature are shown in Fig. 2. The curie temperature for this particular ferroelectric material is 115.75°C. This can be seen in Fig. 2 as the temperature at which the dielectric constant has its maximum value.

Curves of the dielectric constant of this material as a function of applied dc electric field are presented in Fig. 3. This data from another sample of the same material is shown so that a comparison can be made between the change in dielectric constant as determined by the RF electric field, and the change in dielectric constant due to the dc electric field. Some limited large signal data on the dependence of the dielectric constant on the RF electric field can be deduced from measurements made on the ferroelectric limiter. Considerably more data on the large signal properties of ferroelectric materials is needed.

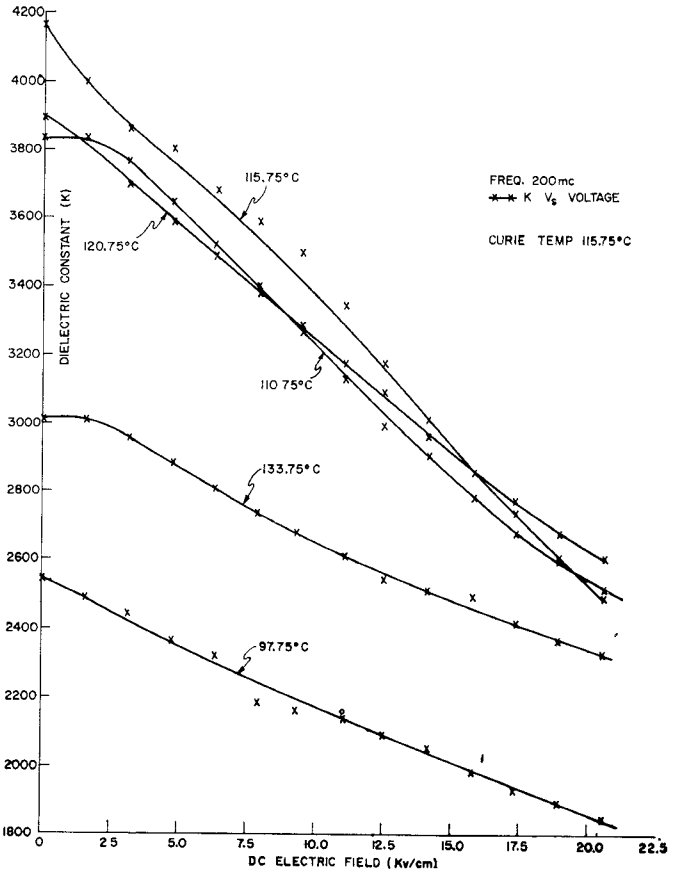

Fig. 3. Dielectric constant vs. direct current voltage.

Limiter Construction

The ferroelectric limiter consists of a symmetrical, loop-coupled, capacity-loaded, coaxial line cavity as shown in Fig. 4. A large portion of the capacity loading is provided by the ferroelectric pellet. Due to the large amount of capacitive loading yielded by the very-high dielectric constant ferroelectric material, the cavity length is well under a quarter wavelength. An electric heater is located outside of the cavity, but near the ferroelectric pellet in order to bring the pellet temperature within a few degrees of its curie temperature. The cavity contains a movable short circuit for resonating it at the desired frequency.

The ferroelectric pellet is in the shape of a circular cylinder of radius r_f and height d_f. The remainder of the capacity loading is essentially an air-filled parallel-plate capacitor of radius $r_a (r_a \gg r_f)$ and height d_a. Figure 4 contains an expanded drawing of the region near the ferroelectric pellet. The pellet is attached to brass rods set in a well of greater spacing than the remainder of the air-filled capacitor ($> d_a$) in order to increase its resistance to high-voltage breakdown. High-voltage breakdown is further retarded by coating the lateral surfaces of the ferroelectric pellet and its supporting brass posts with corona dope. These brass posts, whose radii are equal to the pellet radius, are the principal means of removing heat from the ferroelectric pellet. The entire assembly is filled with sulphur hexafluoride gas (SF_6) at an absolute pressure of one atmosphere.

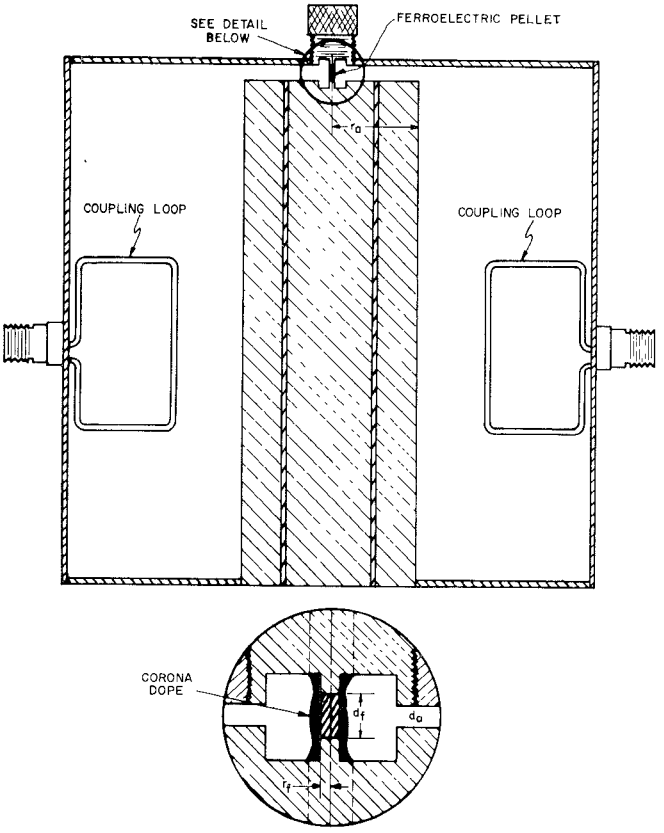

Fig. 4. Ferroelectric limiter configuration.

Principle of Operation

At low-power levels, the limiter acts as a low insertion loss transmission cavity tuned to the signal frequency. As the power level increases, the high RF electric fields developed within the cavity cause the dielectric constant of the ferroelectric pellet to change, thus detuning the cavity. The detuned cavity causes most of the incoming power to be reflected at the input port. Similar reflections at the output port result in increased dissipative losses within the cavity.

Starting with the following well-known equation for the transmission factor (γ) of a cavity,[1]

$$\gamma(P) = \frac{\gamma_0}{1 + Q_L^2\left(\frac{f}{f_0} - \frac{f_0}{f}\right)^2} = \frac{\gamma_0}{1 + Q_L^2\left[\left(\frac{f}{f_0}\right)^2 + \left(\frac{f_0}{f}\right)^2 - 2\right]} \tag{1}$$

an approximate analysis of the performance of the ferroelectric limiter can be performed. In the above equation, the symbols have the following meaning:

$\gamma(P) \leq 1$ is the power transmission factor, which is a function of the RF electric field intensity in this application.

$\gamma_0 \leq 1$ is the power transmission factor at low RF power levels.

Q_L is the loaded Q of the cavity.

f is the signal frequency.

f_0 is the resonant frequency of the cavity.

$$f_0^2 = \frac{1}{4\pi^2 L(C_a + C_f)} \tag{2}$$

where L is the inductance due to the length of short-circuited coaxial transmission line, and C_a and C_f are, respectively, the values of capacitive loading due to the air-filled and ferroelectric-filled end loading. The ferroelectric capacitor is assumed to have the following functional dependence on the magnitude of the RF electric field intensity.

$$C_f = C_0 - \Delta C = \epsilon_0 K \frac{A_f}{d_f} - \epsilon_0 K_1 \frac{A_f}{d_f} \left| E_{\mathrm{RF}} \right| \tag{3}$$

$$C_a = \epsilon_0 \frac{A_a}{d_a} \tag{4}$$

A_f, d_f, A_a, and d_a are the areas and heights of the ferroelectric-filled and air-filled parallel-plate capacitor regions. In this approximate analysis, fringe fields are neglected. From (2), (3), and (4),

$$f_0^2 = \frac{1}{4\pi^2 L(C_a + C_0 - \Delta C)} \tag{5}$$

The signal frequency, which equals the resonant frequency at low-power levels, is given by

$$f^2 = f_0^2(E_{\mathrm{RF}} = 0) = \frac{1}{4\pi^2 L(C_a + C_0)} \tag{6}$$

therefore,

$$\left[\frac{f}{f_0}\right]^2 = 1 - \frac{\Delta C}{C_a + C_0} \tag{7}$$

and

$$\left(\frac{f_0}{f}\right)^2 = \frac{1}{1 - \frac{\Delta C}{C_a + C_0}} \tag{8}$$

Equation (8) can be rewritten in the following form:

$$\left(\frac{f_0}{f}\right)^2 = 1 + \sum_{u=1}^{\infty}\left[\frac{\Delta C}{C_a + C_0}\right]^u \tag{9}$$

therefore,

$$\gamma(P) = \frac{\gamma_0}{1 + Q_L^2 \sum_{u=2}^{\infty}\left[\frac{\Delta C}{C_a + C_0}\right]^u} \tag{10}$$

The RF electric field appearing across the ferroelectric capacitor is related to the available input power from the generator (P_{in}) by the following equation:[1]

[1] Montgomery, C. G., R. H. Dicke, and E. M. Purcell, Principles of microwave circuits. M.I.T. Rad. Lab. Ser., No. 8, ch. 7.

$$E_{RF} = \frac{n}{d_f}\sqrt{4P_{in}Z_0} \tag{11}$$

where Z_0 is the characteristic impedance of the input and output transmission lines, and n is the equivalent transformer turns ratio of the input and output coupling loops. The equivalent turns ratio (n) is related to the cavity coupling coefficient (β), and the equivalent shunt resistance of the unloaded cavity (R_f) by the following equation:[1]

$$n = \sqrt{\frac{R_f}{\beta Z_0}} \tag{12}$$

This shunt resistance is assumed to be totally due to dielectric losses within the ferroelectric pellet. Therefore,

$$R_f = \frac{1}{2\pi f C_f \tan\delta} \tag{13}$$

In this approximate analysis, both β and R_f are assumed to be independent of E_{RF}. The low-power transmission factor γ_0 is related to the coupling coefficient by the following well-known relationship:

$$\gamma_0 = \frac{4\beta^2}{(1-2\beta)^2} \tag{14}$$

$$\gamma(P) = \frac{\gamma_0}{1 + Q_L^2 \sum_{u=2}^{\infty}\left[\frac{2n\Delta C(Z_0)^{1/2}(P_{in})^{1/2}}{(C_a + C_0)d_f}\right]^u} \tag{15}$$

For

$$\frac{2n\Delta C(Z_0)^{1/2}(P_{in})^{1/2}}{(C_a + C_0)d_f} \ll 1$$

which is the case for the ferroelectric material used ($K_1 \ll K$), and the input power levels studied, only the first term of the series need be retained. Therefore,

$$\gamma(P) = \frac{\gamma_0}{1 + Q_L^2\left[\frac{2n\Delta C}{(C_a + C_0)d_f}\right]^2 Z_0 P_{in}} \tag{16}$$

Let

$$P_c = \left\{\left[\frac{2nQ_L\Delta C}{(C_a + C_0)d_f}\right]^2 Z_0\right\}^{-1} \tag{17}$$

therefore

$$P_{out} = \gamma(P)P_{in} = \frac{\gamma_0 P_{in}}{1 + \frac{P_{in}}{P_c}} \tag{18}$$

For $P_{in} \ll P_c$, (18) reduces to the usual linear function.

$$P_{out} = \gamma_0 P_{in} \quad (P_{in} \ll P_c) \tag{19}$$

For $P_{in} \gg P_c$ (18) shows that the output power reaches a constant saturation level.

$$(P_{out})_{sat} = \gamma_0 P_c \quad (P_{in} \gg P_c) \tag{20}$$

For $P_{in} = P_c$, which could be called a corner power level,

$$P_{out} = \frac{\gamma_0 P_c}{2} = \frac{(P_{out})_{sat}}{2} \quad (P_{in} = P_c) \tag{21}$$

Some measured P_{out} vs. P_{in} curves for this type of limiter are presented in Figs. 5 and 6. The shape of these curves illustrate the type of behavior predicted by (18). Equations (17) and (18) indicate how the performance of these limiters can be adjusted through control of the geometry (A_f, A_a, d_a, d_f), coupling coefficient and loaded Q of the cavity (β, n, Q_L).

From measurements of $(P_{out})_{sat}$ and the value of K as determined from small signal measurements, one can determine the value of K_1 and, hence, the large signal value of the dielectric constant as a function of E_{RF}. Measurements on two limiters have yielded the following values of large signal dielectric constant:

$$\epsilon(E_{RF}) = \epsilon_0(4806 - 1.96 \times 10^{-4}|E_{RF}|)$$

and

$$\epsilon(E_{RF}) = \epsilon_0(4806 - 3.82 \times 10^{-4}|E_{RF}|)$$

Where E_{RF} is given in volts per meter. The difference between the two values of K_1 measured on two different pellets of nominally the same material may be due, in part, to different operating temperatures of the pellets. The temperature rise of the pellets due to RF power dissipation is discussed.

Some previous large signal measurements[2,3] made on a different ceramic ferroelectric material at higher frequencies have shown that the instantaneous dependence of the dielectric constant on E_{RF} is of the form, $\epsilon = \epsilon_0(a - bE_{RF}^2)$. The above quadratic functional dependence on E_{RF}, however, results in a calculated power-out vs. power-in characteristic, which reaches a maximum value and then decreases again. An excellent fit with experimental data was obtained through the assumed use of an effective large signal dielectric constant which varies linearly with $|E_{RF}|$.

Temperature Rise and Thermal Relaxation

It is well known that the change of the dielectric constant of ferroelectric materials as a function of dc electric field intensity is dependent on temperature. Although very little data is available on the large signal properties of ferroelectric materials, it is likely that the change of dielectric constant as a function of the RF electric field intensity is similarly temperature dependent. In order to obtain proper operation of the limiter,

[2] Johnson, D. A., Microwave properties of ceramic nonlinear dielectrics, Microwave Lab. Rept. No. 825, Contract No. AF 49(638)-514, Stanford University, Calif., Jul 1961.

[3] DiDomenico, M., D. A. Johnson, and R. H. Pantell, A ferroelectric harmonic generator and the large signal microwave characteristics of a ferroelectric ceramic, Internal Memo. M.L. No. 862, Stanford University, Oct 1961.

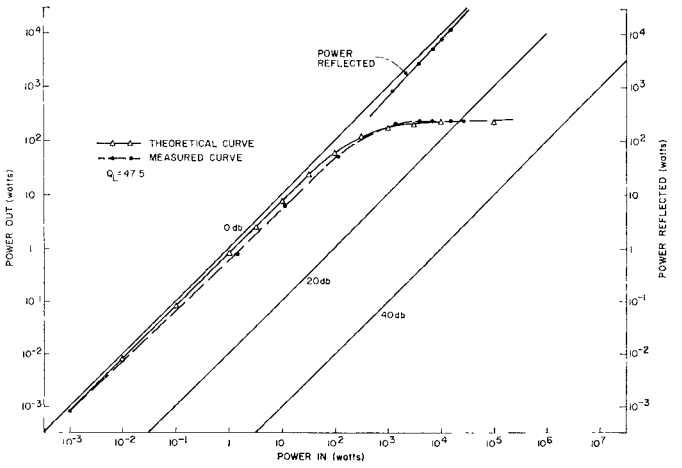

Fig. 5. Ferroelectric limiter characteristics—$Q_L = 47.5$.

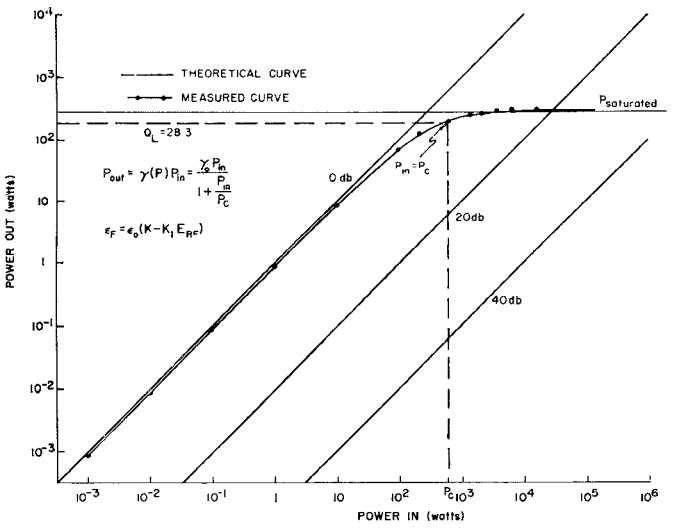

Fig. 6. Ferroelectric limiter characteristics—$Q_L = 28.3$.

it is essential that the ferroelectric pellet be maintained within the proper temperature interval (close to the curie temperature) despite the fact that RF power is dissipated in the pellet. An excessive temperature rise within the pellet will cause the limiter cavity to be detuned. It is essential to the operation of the limiter that the detuning be due to high electric field intensity rather than a temperature change for the following reasons:

1) To obtain rapid response in order to avoid spike leakage.
2) To achieve rapid recovery so that a low-level signal following shortly after the high-power pulse is not attenuated.

In order to estimate both the expected temperature rise due to RF dissipation and the thermal response time of the limiter, an idealized analysis was performed. The specific heat (C_p) and density (ρ) of two different batches of the ferroelectric material were measured and used in this analysis. The pertinent properties of these two materials are shown in Table I. The analysis of the

TABLE I

Ferroelectric material	UR 5324	UR 5359
Constituents	45% $PbTiO_3$ 55% $SrTiO_3$	45% $PbTiO_3$ 55% $SrTiO_3$
Firing temperature	1272°C	1230°C
Curie temperature (T_c)	115.75°C	118°C
Specific heat (C_p) (cal./g°C)	0.15 ± 0.02	0.11 ± 0.02
Density (ρ) (g/cm³)	5.54 ± 0.01	5.53 ± 0.01

thermal system assumes that initially the ferroelectric pellet is at the same temperature (T) as the cavity. The only source for differential heating of the pellet is the RF power dissipated P_d within it. Heat can be transferred from the ferroelectric pellet to the remainder of the cavity only via conduction through the metal posts which contact the circular faces of the pellet. The pertinent parameters of the posts are their thermal conductivity (k), cross-sectional area ($A = \pi r_f^2$), and their length (s).

The heat energies introduced (q_{in}), and extracted (q_{out}) from the ferroelectric pellet are

$$q_{in} = P_d t \tag{22}$$

and

$$q_{out} = \frac{kA}{s} \Delta T t \tag{23}$$

where ΔT is the temperature rise of the pellet, and t is the time measured from the instant when the RF power is applied. The incremental energy stored in the pellet (q_{stored}) is

$$q_{stored} = mC_p \Delta T \tag{24}$$

where m and C_p are the mass and specific heat of the pellet. The heat balance equation requires that

$$q_{in} - q_{out} = q_{stored} \tag{25}$$

therefore,

$$\Delta T = \frac{P_d t}{mC_p + \frac{kA}{s} t} \tag{26}$$

The equilibrium temperature rise is given by the following equation:

$$\lim_{t \to \infty} \Delta T = \frac{sP_d}{kA} \tag{27}$$

Let

$$\Delta T(t) = r(sP_d/kA) \tag{28}$$

where $0 \leq r \leq 1$, and is the ratio of the instantaneous temperature rise to the final equilibrium temperature rise. From (26) and (28), an expression for the time required for the ferroelectric pellet to reach any fraction of its final equilibrium temperature rise is obtained.

$$t_r = \frac{smC_p}{kA} \cdot \frac{r}{1-r} \tag{29}$$

The time required to reach half of its final value ($r=0.5$) is

$$t_{0.5} = \frac{smC_p}{kA} \tag{30}$$

Using the proper material constants and geometric parameters, the half time ($t_{0.5}$) for a limiter containing a pellet of UR 5324 can be calculated.

$r_f = 0.0165$ inch
$d_f = 0.080$ inch
$s = 0.035$ inch $= 0.089$ cm
$A = 2A_f$ (two posts) $= 2\pi(r_f)^2 = 1.102 \times 10^{-2}$ cm^2
$k = 0.26$ cal/cm-sec-°C (brass)
$C_p = 0.15$ cal/g-°C
$\rho = 5.54$ g/cm^3
$\therefore m = \rho A_f d_f = 6.2 \times 10^{-3}$ g
$\therefore t_{0.5} = 28.9$ ms

The above measure of the response time is very long compared to typical pulse lengths (τ_p) of high-power systems. For $t \leq \tau_p \ll t_{0.5}$, (26) can be approximated as follows:

$$\Delta T = \frac{P_d}{mC_p} t \tag{31}$$

Thus, at the end of the first pulse ($t=\tau_p$), the pellet temperature will have risen an amount α given by

$$\alpha = \frac{P_d \tau_p}{mC_p} \tag{32}$$

At the cessation of the pulse, the pellet temperature decreases according to the following relationship:

$$\Delta T = \frac{\alpha}{1 + t/t_{0.5}} \tag{33}$$

During the time interval between pulses (θ), ΔT will decrease but will not reach zero. It will decrease to a value given by

$$\Delta T = \beta = \frac{\alpha}{1 + \theta/t_{0.5}} \qquad (\text{at } t = \tau_p + \theta) \tag{34}$$

After successive intervals of τ_p and θ, the temperature difference will follow a sequence as listed in Table II.

After steady state has been reached ($l \to \infty$), the pellet temperature will vary between the limits determined by the sum of the geometric series listed in Table II. At $t = l\tau_p + (l-1)\theta$:

TABLE II

t	ΔT
0	0
τ_p	α
$\tau_p + \theta$	$\alpha\left[\frac{1}{1 + (\theta/t_{0.5})}\right]$
$2\tau_p + \theta$	$\alpha + \alpha\left[\frac{1}{1 + (\theta/t_{0.5})}\right]$
$2\tau_p + 2\theta$	$\alpha\left[\frac{1}{1 + (\theta/t_{0.5})}\right] + \alpha\left[\frac{1}{1 + (\theta/t_{0.5})}\right]^2$
$l\tau_p + (l-1)\theta$	$\alpha \sum_{u=0}^{l-1} \left[\frac{1}{1 + (\theta/t_{0.5})}\right]^u$
$l\tau_p + l\theta$	$\alpha \sum_{u=1}^{l} \left[\frac{1}{1 + (\theta/t_{0.5})}\right]^u$

$$\Delta T = (\Delta T)_{\max} = \alpha\left[\frac{t_{0.5}}{\theta} + 1\right] = \frac{P_d \tau_p s}{kA\theta} + \frac{P_d \tau_p}{mC_p} \tag{35}$$

at $t = l\tau_p + l\theta$

$$\Delta T = (\Delta T)_{\min} = \alpha \frac{t_{0.5}}{\theta} = \frac{P_d \tau_p s}{kA\theta} \tag{36}$$

In the case of the previously discussed limiter configuration having a response time of 28.9 ms, it was found that a peak power input of 26.3 kW resulted in reflected and transmitted power levels of 23.4 kW and 0.22 kW, respectively. The peak power dissipated (P_d) was thus 2.68 kW (640 cal/s). It will be assumed that all of this power was dissipated within the ferroelectric pellet. For the case cited, $\tau_p = 8 \times 10^{-6}$ s, and $\theta = 16.67 \times 10^{-3}$ s (60 pulses per s). Using (35) and (36), it is found that

$$(\Delta T)_{\min} = 9.55°\text{C}$$

and

$$(\Delta T)_{\max} = 15.05°\text{C}$$

In order that the ferroelectric pellet be at a temperature near its curie temperature (T_c) at the cessation of a pulse (after steady-state conditions have been reached), the ambient temperature of the cavity should be maintained at a temperature near

$$T = T_c - (\Delta T)_{\max}$$

Since K_1 is largest in the vicinity of the curie temperature, spike leakage will be minimized, if the temperature rise during the pulse $[(\Delta T)_{\max} - (\Delta T)_{\min}]$ is minimized. Equation (36) shows that this can be accomplished through the use of a heavier ferroelectric pellet. The above example indicates that recovery time is not a

problem, since the pellet temperature will change very little during an interval of a few milliseconds following cessation of the high-power pulse.

Measured Results

The small signal frequency response of the limiter is shown in Fig. 7. Each of these curves is for a different coupling loop size and, hence, a different coupling coefficient β. These measurements provided information on the coupling loop configurations needed to obtain desired values of small signal insertion loss γ_0, and loaded $Q(Q_L)$. Similar measurements were made at various temperatures, and they showed that a low insertion loss can be maintained over a temperature range of a few degrees in the vicinity of the curie temperature T_c.

Using the measured values of γ_0 and Q_L, β and the unloaded $Q(Q_u)$ can be calculated. The value of Q_u in conjunction with C_a/C_f, as determined from the geometry and small signal dielectric constant measurement, allows one to compute the loss tangent (tan δ) of the ferroelectric material. The value of tan δ as determined from a number of cavity measurements at the curie temperature is 0.0037.

High-power measurements, made on limiters containing these small ferroelectric pellets, indicated that the desired limiting action could be obtained, but high-voltage breakdown occurred at input power levels of 10 kW or less. When the pellet height d_f was increased to 0.080 inch, it was found that input power levels up to 26.3 kW (the maximum power available for testing) could be handled without adverse effects. Small signal measurements on this limiter showed that the insertion loss γ_0 was 0.85 dB and the loaded Q was 47.5. The measured P_{out} vs. P_{in} curve of this limiter is shown in Fig. 5. The reflected power is also shown. The measured output power at saturation $(P_{out})_{sat}$ is 224 watts. Using this value of $(P_{out})_{sat}$ and (16), K_1 was determined to be 1.96 by 10^{-4} meters/volt. This value of K_1 was inserted in (17) and (18) to compute the theoretical P_{out} vs. P_{in} curve shown on Fig. 5. It should be noted that the theoretical curve was forced to agree with the measured curve at saturation. The two curves have the same form at lower power levels. This agreement appears to confirm the assumed dependence of the dielectric constant on the RF electric field intensity.

In order to reduce the low-level insertion loss and increase the power handling capability by decreasing the internal RF electric field, the coupling coefficient was increased. This was accomplished by using two turn loops at both the cavity input and output. The low-level insertion loss was thereby decreased to 0.5 dB and the loaded Q reduced to 28.3. The measured P_{out} vs. P_{in} curve of this final limiter is shown on Fig. 6. The measured $(P_{out})_{sat}$ of 300 watts indicates that K_1 was 3.82 by 10^{-4} meters/volt. The discrepancy between the two values of K_1 may be due to different pellet temperatures. More extensive large signal measurements are needed to determine K_1 as a function of temperature. The measured and theoretical limiter characteristics shown in Fig. 6 are in nearly perfect agreement.

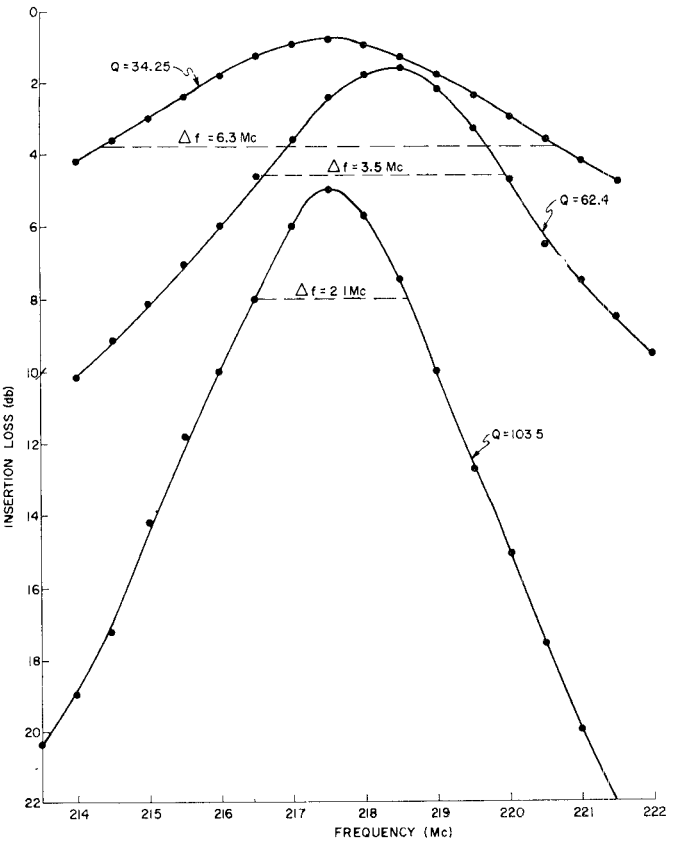

Fig. 7. Frequency response of ferroelectric-loaded cavity.

Additional measurements were made on the ferroelectric limiter in order to obtain recovery time data. An interlaced train of high-power and low-power pulses were injected into the limiter. The high- and low-power pulses were from separate signal generators. The low-power pulse was triggered by the high-power pulse through a variable delay line. In this manner, the time interval between the trailing edge of the high-power pulse and the leading edge of the low-power pulse could be varied continuously. Fig. 8 is an oscilloscope photograph which shows the combined high-power, low-power signals as they emerge from the limiter. In this picture, time is increasing to the left, and amplitude is increasing downward. Determination of the recovery time was made by varying the time delay thus moving the low-power pulse into the trailing edge of the high-power pulse until the former was no longer discernible. This measurement indicated that the limiter had a recovery time of less than 10 μs. The sweep time calibration for the oscilloscope was set at 20 μs per division. It should be pointed out that from the calculations shown previously, the thermal time constant was on the order of 28.9 ms. If the nonlinear effects of the ferroelectric material were due mainly to a change in temperature rather than a change in RF electric field intensity, the low-power pulse would not be seen within the time base of the oscilloscope photograph of Fig. 8.

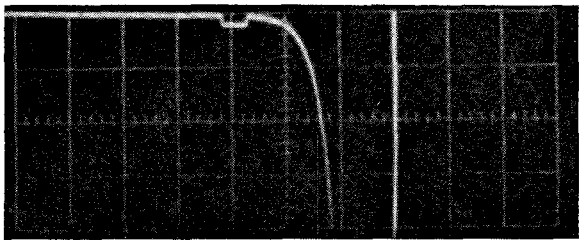

Fig. 8. Output of limiter showing low-power and high-power pulses.

Conclusions

It has been shown that the large signal nonlinear properties of ferroelectric materials can be used to obtain power limiting. A ferroelectric limiter capable of handling peak input power levels in excess of 25 kW, while yielding a saturated output power level of 300 watts with a small signal insertion loss of 0.5 dB has been built. A theoretical analysis, which accounts for the observed limiting action, indicates that power levels of several megawatts can be handled with suitably mounted ferroelectric pellets that can be conveniently fabricated. Even greater power handling capability can be expected if the ferroelectric material is used in a traveling-wave resonator configuration like that previously used to design a ferroelectric phase shifter.[4,5]

Additional data on the large signal properties of ferroelectric materials, particularly their temperature dependence, is needed. The limited available material data indicates that ferroelectric limiters will offer their greatest advantage in the HF, VHF, and UHF bands.

It should be noted that the structure used for the high-power ferroelectric limiter can readily be adopted for use as a high-power switch or an electronically tunable filter.

[4] Cohn, M., and A. F. Eikenberg, UHF ferroelectric phase shifter research, Res. Div. Electronic Communications, Inc., Timonium, Md., Final Rept on Contract No. AF 19(604)-8379, April 30, 1962.

[5] Cohn, M., and A. F. Eikenberg, Ferroelectric phase shifters for VHF and UHF, *IRE Trans. on Microwave Theory and Techniques*, vol MTT-10, Nov 1962, pp 536–548.

E- and *H*-Plane Bends for High-Power Oversized Rectangular Waveguide

JOHN P. QUINE, MEMBER, IEEE

Abstract—A study is presented of theoretical and experimental results of *E*- and *H*-plane bends for high-power oversized rectangular waveguide having cross-section dimensions in the range between 1.5 and 2.5 free space wavelengths. It is expected that waveguides having these dimensions will be able to transmit 50 to 100 kW of average power at *X*-band without water cooling. The transmission of at least 5.0 MW of peak power at *X*-band without pressurization is also a design objective.

Dimensions for bends having low-mode conversion loss were determined by numerical integration of the coupled transmission line equations. The dominant $TE_{10}^{\square}$ mode and four spurious modes were considered in these calculations. The results obtained for both constant curvature and sinusoidally shaped *E*- and *H*-plane bends are presented.

A compact *H*-plane constant curvature bend is described for which the ratio of centerline radius to waveguide width is equal to 1.48. The measured mode conversion loss to the $TE_{20}^{\square}$, $TE_{30}^{\square}$, and $TE_{40}^{\square}$ modes for an experimental model having a width equal to 2.25 inches was less than −20 dB in the frequency range from 7.0 to 11.0 Gc/s.

Manuscript received June 15, 1964; revised November 2, 1964. The work was supported by the Rome Air Development Center under Contract AF 30(602)-2990 with the General Electric Company, Heavy Military Electronics Department.

The author is with Advanced Technology Laboratories, General Electric Company, Schenectady, N. Y.

Introduction

THE PRACTICAL realization of reliable oversized waveguide systems for high-power applications depends on the development of components having low-energy conversion to spurious propagating modes. An important advantage of rectangular waveguide in the design of components, such as bends, is the absence of modes which are degenerate with the desired $TE_{10}^{\square}$ mode. The bend study outlined here is part of a general study to develop a whole family of components compatible with rectangular waveguides of the stated dimensions.

Dimensions for bends having low-mode conversion loss were determined by numerical integration of the coupled transmission line equations. The dominant $TE_{10}^{\square}$ mode and four spurious modes were considered in these calculations. Theoretical results are presented for both constant curvature and sinusoidally shaped *E*- and *H*-plane bends. Experimental results are presented for constant curvature *H*-plane bends.

Constant Curvature Bends

A waveguide bend can be represented by *n*-coupled